Effect of nonlinearity induced by atomic switch in Ag/Ag$_2$S nanoparticles on performance of in-materio reservoir computing

Thien Tan Dang ; Oradee Srikimkaew ; Deep Banerjee ; Saman Azhari ; Yuki Usami ;
Hirofumi Tanaka ✉

Check for updates

CHORUS

View Online

Export Citation

22 July 2024 06:37:51

Effect of nonlinearity induced by atomic switch in Ag/Ag$_2$S nanoparticles on performance of in-materio reservoir computing

View Online   Export Citation   CrossMark

Thien Tan Dang,[1,2,3] (iD) Oradee Srikimkaew,[1] (iD) Deep Banerjee,[1,4] (iD) Saman Azhari,[1,4,a)] (iD) Yuki Usami,[1,4] (iD)
and Hirofumi Tanaka[1,2,3,4,b)] (iD)

AFFILIATIONS

[1]Graduate School of Life Science and Systems Engineering, Kyushu Institute of Technology (Kyutech), 2-4 Hibikino, Wakamatsu, Kitakyushu 808-0196, Japan

[2]Faculty of Applied Science, Ho Chi Minh City University of Technology (HCMUT), 268 Ly Thuong Kiet Street, District 10, Ho Chi Minh City, Vietnam

[3]Vietnam National University Ho Chi Minh City, Linh Trung Ward, Thu Duc District, Ho Chi Minh City, Vietnam

[4]Research Center for Neuromorphic AI Hardware, Kyushu Institute of Technology (Kyutech), 2-4 Hibikino, Wakamatsu, Kitakyushu 808-0196, Japan

a)**Present address:** Graduate School of Information, Production and Systems, Waseda University, 2-7 Hibikino, Wakamatsu, Kitakyushu, Fukuoka 808-0135, Japan.
b)**Author to whom correspondence should be addressed:** tanaka@brain.kyutech.ac.jp

ABSTRACT

A random network of Ag/Ag$_2$S nanoparticles (NPs) was used as a physical system in reservoir computing (RC) because the network has nonlinear and dynamical characteristics. Ag/Ag$_2$S NPs were synthesized by the modified Brust–Schiffrin method. Atomic switching among the NPs caused nonlinear dynamical behavior of the random network. The Fourier transform of output signals indicated that the generated harmonics were far higher with a larger amplitude of the input sine wave because the atomic switching occurred only at high bias voltages. Higher accuracy was achieved in the Boolean logic RC task because of the nonlinearity originating from switching. These findings suggest that nonlinearity plays a fundamental role in the design and implementation of RC devices.

Reservoir computing (RC)—a subclass of recurrent neural networks (RNNs) suitable for spatiotemporal information processing[1]—has recently become a promising route for realizing physical-based neural network hardware. Compared with conventional RNNs, RC offers a faster machine-learning approach because only the readout weights are trained to fit the target, whereas the randomly connected nonlinear reservoir network and weights are unregulated.[2] The dynamical behavior of reservoir networks can be advantageously implemented in hardware using various physical systems.[3] Any system capable of exhibiting nonlinear dynamic responses can function as a reservoir.[4] Physical system resources include mechanics,[5] spintronics,[6,7] photonics,[8,9] nanomaterials,[10–17] and quantum systems.[18] Among these, functional nanomaterials are promising to owe to their ability to form large-scale complex networks with unique dynamics in highly integrated devices.[19–23]

Our previous work reported the synaptic-like behavior and RC applications of a randomly connected Ag/Ag$_2$S nanoparticles (NPs) network.[24] By modulating the input pulse width and interval, the formation and annihilation of metallic bridges between nanoparticles based on the atomic switching phenomenon were controlled, which emulated the potentiation and depression of synapses. Furthermore, demonstrated by voltage–time analysis, the Ag/Ag$_2$S NPs device was suitable as the reservoir layer because of its nonlinearity with higher harmonic generation and phase-shift properties.[25] However, Ag/Ag$_2$S NP-based RC still needs to be clarified, for example, the role of the nonlinear dynamics induced by an atomic switch in high-performance information processing.

Therefore, in this study, we experimentally realized RC via the detection of multiple signals from Ag/Ag$_2$S core–shell NPs random networks to investigate the role of nonlinear dynamics.

22 July 2024 06:37:51

The signal dynamics and nonlinearity were examined according to the interaction between the electric field and the migration of Ag ions involved in atomic switching. The nonlinear dynamics were evaluated by changing the intensity of the electric field (bias voltage). A comparative fast Fourier transform (FFT) analysis of the voltage–time curves confirmed that stronger dynamic nonlinear behavior was generated by the higher bias voltage, and the stronger nonlinearity from the higher bias voltage improved the information processing performance for a sine-wave approximation task. Furthermore, we verified the impact of nonlinear dynamics on the performance of more practical and complex RC tasks, such as Boolean logic reconstruction.

Ag/Ag$_2$S core–shell NPs were synthesized at room temperature using a modified Brust–Schiffrin procedure,[26,27] as shown in Fig. 1(a). An aqueous solution of AgNO$_3$ (200 mg, 99.0% purity, Sigma-Aldrich) was mixed with a toluene solution of tetraoctylammonium bromide (360 mg, 98.0% purity, Sigma-Aldrich) and allyl mercaptan (AM) (0.37 ml, 80% purity, Tokyo Chemical Industry) under magnetic stirring for 30 min. Subsequently, after the removal of water phase, a deionized water solution of an NaBH$_4$ reducing agent (260 mg, 95% purity, Tokyo Chemical Industry) was added to the mixture.
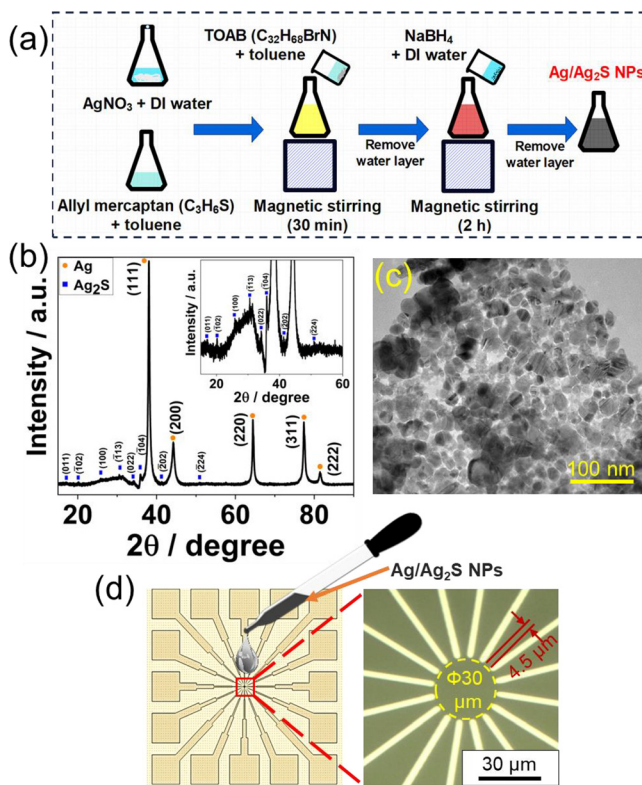
FIG. 1. Fabrication process and material characterization of Ag/Ag$_2$S NPs. (a) Graphical synthesis procedure of Ag/Ag$_2$S NPs. (b) XRD pattern and (c) TEM image obtained from fabricated NPs, whose average diameter was 34 ± 10 nm. (d) Ag/Ag$_2$S NP in-materio RC device fabricated by drop-cast of the NPs to substrate having 16-electrodes array produced by photolithography. The right figure shows an optical microscopy image of the electrode array around the center gap region with a 30-μm diameter. The distance between the closest electrodes was approximately 4.5 μm.

The reduction reaction proceeded under constant stirring for 2 h. Finally, water phase was removed again, and then, ethanol was added to the toluene phase with obtained product to remove the excess AM from toluene solution. Then, the solution was centrifuged at 4000 rpm for 20 min to pick the precipitation up as a target product.

The synthesized product was characterized via x-ray diffraction (XRD) and transmission electron microscopy (TEM) to confirm the presence of Ag/Ag$_2$S NPs. The main peak in the XRD pattern is attributed to Ag and Ag$_2$S, as shown in Fig. 1(b), indicating that Ag and Ag$_2$S coexisted in the obtained product. The shape of NPs was spherical observed by TEM as shown in Fig. 1(c). The average particle diameter was 34 ± 10 nm. The results confirmed that Ag/Ag$_2$S NPs were fabricated.

A 16-electrode device was fabricated on an Si/SiO$_2$ wafer using maskless photolithography (DDB-701-DL, NEOARK) in an electrode pad region with a Ti/Pt 6 nm/24 nm electrode thickness via sputtering (SPC-350, Eiko). A circular gap was fabricated with a 30-μm diameter at the center of the electrode array, and the distance between the closest electrodes was 4.5 μm, as shown in Fig. 1(d). The in-materio RC device was formed by drop-casting 5 μl of the ethanol suspension of the synthesized Ag/Ag$_2$S NPs onto the center of the electrodes, while they were placed on a hotplate set at 50 °C for ethanol evaporation. A chip package was fabricated for the device using a printed circuit board, and each electrode was connected to a pin via wire bonding. Hence, multiple output electrodes could be recorded simultaneously to investigate the dynamic computing inside a reservoir.

Current–voltage (I–V) measurements were performed using a semiconductor parameter analyzer (Agilent 4156 B). The Ag/Ag$_2$S NPs device was connected via two probes to extract the electrical responses, and a personal computer wired to a semiconductor parameter was used to control the measurement procedure with the LabVIEW program. The electrical properties were investigated by applying a bias voltage to the device. The bias was repeatedly swept forward and reversed from 0 to 4 V in steps of 0.02 V per second. To evaluate the effects of the bias-voltage range on the electrical properties, a cycle bias in the range of −4 to 4 V was applied to the Ag/Ag$_2$S NPs device with 0.02-V steps in each second. The compliance current was set to 1 mA to prevent device damage. Electrochemical impedance spectroscopy (EIS) was performed using a Solartron 1260 impedance analyzer with a dielectric constant measurement interface (Solartron 1296) at AC 0.3 V in the frequency range of 1 MHz to 0.1 Hz.

The experimental setup and learning algorithm for the RC tasks were identical to those used in our previous studies.[12,20,28] A multifunction data-acquisition (DAQ) system (PXIe-6363, National Instruments) was used for input signal generation, and output data were recorded using a custom LabVIEW program. All the equipment and devices were grounded. Fifteen output responses were collected in parallel over 60 s using a multifunction DAQ system. For in-materio reservoir operation, 80% of the data were used for training, and 20% were used for testing.

As shown in Fig. 2(a), a nonlinear response with a gradually increasing output current was observed. In Ag/Ag$_2$S NPs, conductive filament formation/annihilation occurs upon the application or removal of a bias voltage.[25] In the first sweep, the current began to increase at 3 V and reached 0.5 mA, allowing the development of Ag filaments among the NPs. During the reverse bias of the first sweep, the output current exhibited a nonlinear response to the forward sweep
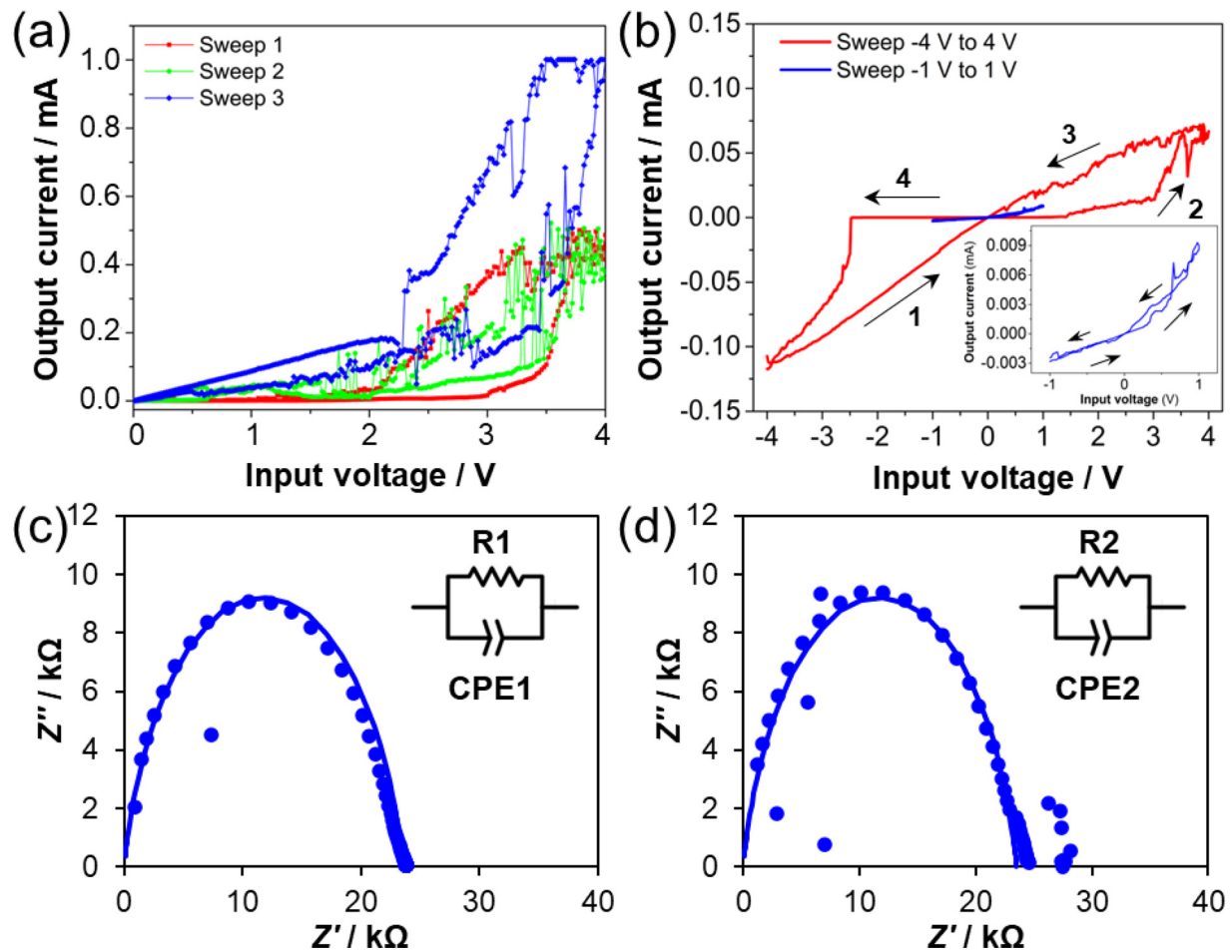
FIG. 2. (a) I–V curves of the device after multiple forward and reverse bias sweeps from 0 to 4 V, which shows a nonlinear response and a gradual increase in the current, indicating the random formation of conduction paths inside the Ag/Ag$_2$S network. (b) Current response after the application of the cycle bias in the ranges of ± 4 V and ± 1 V (inset). (c) and (d) Nyquist plots obtained by EIS at DC 0 V and DC 3 V, respectively. Z$'$ and Z$''$ indicate the real and imaginary parts of the impedance, respectively. The dots indicate experimental data, and the solid lines are the fitting curves obtained from the CPE-R equivalent circuits shown in the insets ($R1 \approx 2.3$ kΩ, $CPE1 \approx 4.3$ nF, $n_{CPE1} \approx 0.847$ and $R2 \approx 2.5$ kΩ, $CPE2 \approx 9.4$ nF, $n_{CPE2} \approx 0.781$).

curve, and the current slowly decreased, indicating filament disintegration. In the second sweep, the output current began to increase at an applied bias voltage of approximately 0.6 V, which was lower than the value for the first sweep. In the third sweep, the output current began to increase at 0.2 V, which was lower than the value for the second sweep. Furthermore, significant current variations occurred in the range of 2–4 V, indicating that the production and destruction of the conduction paths among the NPs network proceeded randomly at various gap sites. The third bias sweep resulted in a gradual increase in the output current up to a compliance current of 1 mA, indicating that a strong connection was generated in the Ag/Ag$_2$S NP network.

The applied voltage creates an electric field that drives the migration of Ag ions across the interface, forming conductive paths or filaments between the Ag core and silver sulfide shell.[29,30] When a bias voltage was applied, the Ag ions in the Ag$_2$S shell were reduced, forming metallic Ag atoms, which gathered on the surface of the Ag$_2$S layer and formed conductive filaments between the NPs. Thus, the conductivity

of the material changed from a high-resistance state to a low-resistance state. Conversely, removing the bias reduced the kinetic driving force, and the Ag atoms in the conductive filaments are oxidized to Ag ions, which migrate back to the Ag$_2$S shell medium. The process causes the conductive filaments to dissolve and the material to return to its high-resistance state.[31] This phenomenon is consistent with the findings of a previous study[32–34] in which researchers demonstrated a filament formation and annihilation mechanism among NP networks, which is essential for high RC performance with electrical nonlinearity.

Moreover, the Ag/Ag$_2$S NPs device switched with pinched hysteresis behavior, as shown in Fig. 2(b). At high applied voltages, the current response exhibited pinched hysteresis with a large ON/OFF ratio (approximately 10^3). In a lower bias range, the ON/OFF ratio was low (approximately 10^0), with almost the same current value, indicating a lower degree of nonlinearity. Switching behavior was observed at approximately 3–4 V in both the negative and positive bias regions, generating the transient dynamic signal characteristic of the network,

which was not observed in the range of ± 1 V. Nonlinear dynamic behavior of Ag/Ag$_2$S NPs is essential for RC because the nonlinear high-dimensional characteristics allow the transformation of input data into multiple higher-order signals, which increases the accuracy of task implementation. Therefore, the volume of the nonlinear dynamic response plays an important role in the data transformation and significantly affects the RC performance.

EIS was performed to further investigate the electrical properties. Figures 2(c) and 2(d) show the Nyquist plots of the Ag/Ag$_2$S NPs device at DC 0 V and DC 3 V. Both plots were fitted using a constant-phase element and resistance (CPE-R) equivalent circuit. The equivalent circuit represented the capacitance and resistance of the conductive filaments formed among the NPs. The Nyquist plots at a high bias (DC 3 V) were unstable, implying that filament growth occurred, and electrical parameters, such as the resistance and capacitance, changed slightly during the EIS measurement. The results coincided with the current response of the first sweep in Fig. 2(a), and with the continuous bias in range of 0–3 V, there was a modestly fluctuation at 3 V, while at lower bias, the current almost maintained. This implies that the atomic switch triggered the formation of filaments had to be above a certain threshold to support this process.

Several studies have generally involved the development of hardware components or devices that can efficiently perform RC tasks such as waveform generation,[11,24,30] spoken digit classification,[13,35] and pattern recognition[17,36] by exploiting the complex nonlinear dynamics of the network. However, while a substantial body of research highlights the brain-liked dynamic behavior of atomic switch networks, there is a noticeable gap in our understanding of how the nonlinear dynamical affects task execution. Here, we performed a sine-wave function approximation task to analyze the degree of nonlinearity in responding to task performance.[37] The sine-wave function allowed control of the degree of nonlinearity ν in the tasks, as follows:

$$y(t) = f(s(t)) = \sin(\nu s(t)), \tag{1}$$

where f, $s(t)$, and ν are a nonlinear function, the input signal, and a task parameter that controls the extent of the required nonlinearity, respectively. To perform the function approximation task, white noise with two uniform distributions, i.e., $\mu_1(-1, 1)$ V and $\mu_2(-4, 4)$ V, was fed to the device as the input signal $s(t)$, where $\mu(x_1, x_2)$ means that the white noise amplitude ranges between x_1 V and x_2 V. The task performance was compared between the two different bias ranges. After weight optimization via training, the test accuracy was calculated from the fitting value between the predicted and target data,

$$Test\ accuracy = \left(1 - \left(\frac{\sum \left(y(t) - z(t)\right)^2}{\sum y(t)^2}\right)\right), \tag{2}$$

where $y(t)$ and $z(t)$ represent the target matrix and predicted reservoir output, respectively. Figure 3(a) presents the results of comparing the test accuracies between μ_1 and μ_2 by changing ν in the range of [0.1, 4.5] with steps of 0.1. As shown, the device exhibited high accuracy ($\geq 95\%$) in both cases for $\nu \leq 2$. When ν value increased from 2 to 3.5, the accuracy decreased sharply to $<50\%$. With a further increase in ν, the accuracy gradually decreased. When ν reached the final value of 4.5, the test accuracy for the input μ_1 was 1.97%, whereas that for μ_2 was higher (21.73%). The FFT of output signals obtained with the input sinusoidal wave (11 Hz) indicated that a higher bias voltage generated higher harmonic frequencies[20,38] (i.e., larger integer multiples of the input sinusoidal wave frequency), as shown in Figs. 3(b) and 3(c). The power spectral densities (PSDs) of higher harmonic frequencies
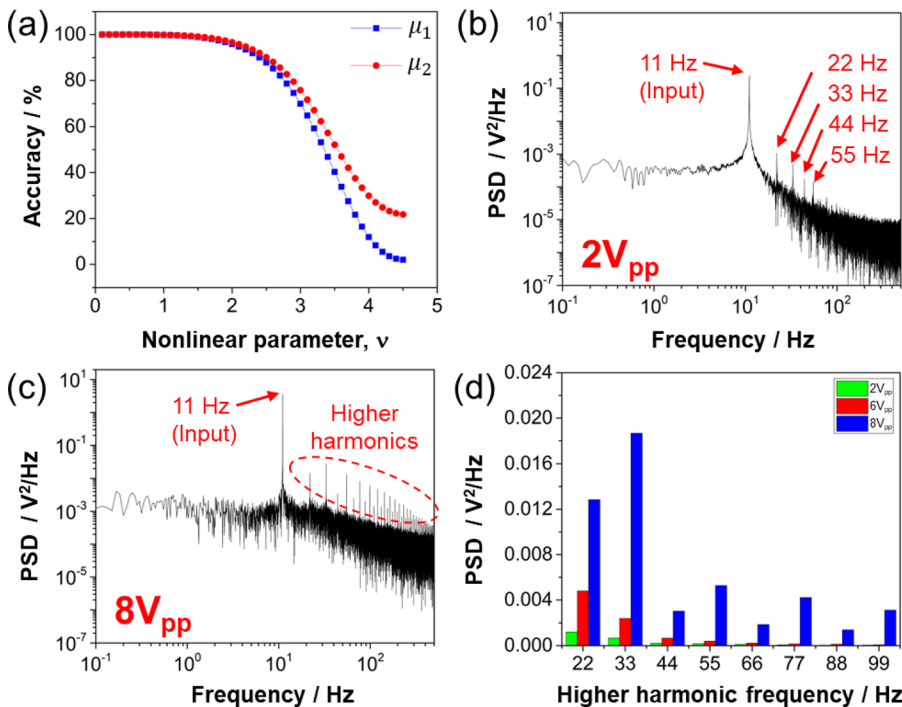

FIG. 3. (a) Comparison of test accuracies between two uniform distribution input ranges—$\mu_1 = \pm 1$ V (blue squares) and $\mu_2 = \pm 4$ V (red circles)—with changing the nonlinear parameter, ν. (b) and (c) PSD vs frequency log–log plots for an input sinusoidal wave (11 Hz) at 2 V$_{pp}$ and 8 V$_{pp}$, respectively. The generated harmonics are indicated by peaks. (d) Comparison of PSD intensities at higher harmonic frequencies ranging from 22 to 99 Hz at 2 V$_{pp}$ (green), 6 V$_{pp}$ (red), and 8 V$_{pp}$ (blue).

with three different bias voltages are shown in Fig. 3(d). These profiles suggest that the random network forms intricate connections and, with its inherent nonlinearity, transforms the input signal into higher-dimensional spatiotemporal outputs.[20] Interpreting the EIS also facilitates an understanding of the dynamics of the system responsible for higher harmonic generation. We extracted the parameter values after fitting each Nyquist plot, as increased the bias, the capacitance is observed to increase, suggesting that with higher bias, a greater amount of charge can be stored in the Ag–Ag$_2$S–Ag junctions for multiple redox reactions. Consequently, there is a decrease in the flow of free carriers, resulting in an elevation in the amplitude of noise, which is in good correspondence with the result in the I–V characteristics presented above, where the device exhibited a higher nonlinearity response in the case of output currents with larger pinched hysteresis for the ± 4 V sweep cycle. The output signals displayed differences in both amplitude and phase similarity when compared to the input, suggesting the capability to generate a wide range of dynamic output responses, thus further highlighting the strength of the nonlinearity that affected the efficiency of the task implementation. This phenomenon is a frequently observed occurrence in diverse nonlinear systems that rely on physical reservoirs.[12,20,38–40]

In addition, we demonstrated the RC task of Boolean logic optimization—a common nonlinear operation utilized in practical computing[28,41] that cannot be solved without nonlinear data transformation.[41] The device was integrated with a measurement system controlled by LabVIEW software. Figure 4(a) shows a flow chart of the Boolean logic optimization. For this operation, two input streams V_{In1} and V_{In2} consisting of "0" and "1" sampled at 1 bit/s were fed to the device, with the frequency of V_{in2} being doubled to create four states of inputs in the form of (0,0), (0,1), (1,0), and (1,1). The outputs from the 14 electrode pads were collected using a multifunction DAQ. These outputs were trained (blue dots) to reconstruct the logic target functions of OR/XOR (black line) using linear regression, as described in a previous study.[28] The task performance was predicted using two different input amplitude streams (red dots). To evaluate the importance of strong nonlinearity for task execution, the binary state 1 was set as 1 and 4 V, while the binary state 0 was fixed at 0 V, as shown in Figs. 4(b)–4(e).

We selected XOR as the logic gate target because of the complexity of nonlinear classifiers. The XOR gate is often used as an example to illustrate the need for nonlinear classifiers in machine learning because it requires a nonlinear decision boundary to be properly represented.[20,42] As shown in Figs. 4(b) and 4(c), the OR gate is linearly separable and simpler than the XOR gate; therefore, the OR gate achieved a higher prediction accuracy (87.1% for the OR target vs 61.7% for the XOR target). Although the training (blue dots) and prediction (red dots) quite followed their respective targets (black line), fluctuations appeared for both gates at the step edges of transitioning from a 0 state to a 1 state, and there was a mismatch in following the horizontal lines at 1 V input bias. At higher bias voltages, the prediction accuracies were significantly higher (94.1% for OR and 84.1% for XOR), as shown in Figs. 4(d) and 4(e). This improved performance is a manifestation of nonlinear dynamical exploitation. When voltages of increased amplitude were applied to the Ag/Ag$_2$S network, chaotic and fluctuating processes occurred because of the diverse redox states among the particle networks, which generated nonlinear responses, as shown in Fig. 2(a). Additionally, Fig. 2(b) indicates that a higher input voltage
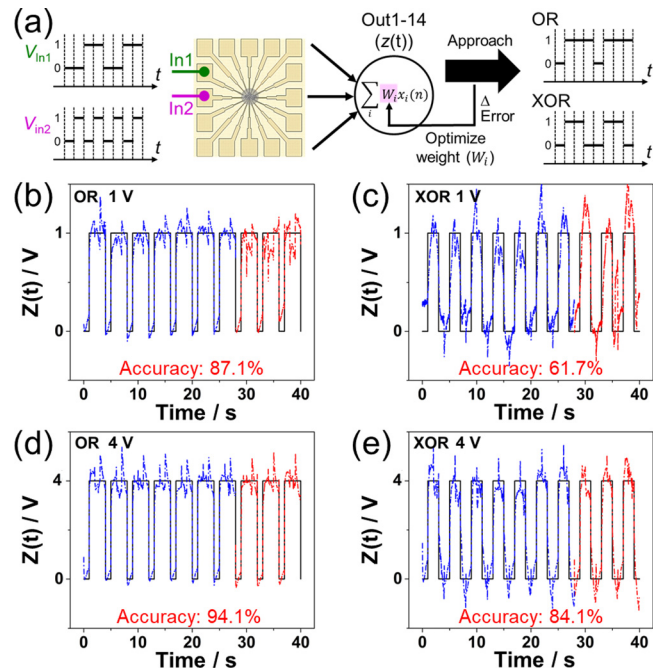
FIG. 4. (a) Flowchart of the Boolean logic optimization task. (b)–(e) Comparison of Boolean logic operation task results of target logic gates OR (left) and XOR (right) between two input conditions. (b) and (c) Input voltage amplitude of 0 V corresponded to the logic state 0, and 1 V corresponded to the logic state 1. (d) and (e) Input voltage amplitude of 0 V corresponded to the logic state 0, and 4 V corresponded to the logic state 1. In these plots, the black solid line, blue dotted line, and red dotted line correspond to the target Boolean logic function, training part, and predicted part, respectively.

caused stronger nonlinearity. Moreover, compared with OR, XOR is linearly inseparable and requires a nonlinear transformation. Hence, the increase in the prediction accuracy for the XOR gate under a higher bias voltage was significant. It is worth noting that the accuracy of the system can be further enhanced by optimizing the stimulation parameters that control the nonlinear response of the physical material networks. These enhancement effects were consistently observed in several functional material reservoir systems, such as modulating the input pulse interval and frequency,[17,24] which cause various network segments to respond nonlinearly differently or create more virtual nonlinear nodes with delay systems[35,43] enriching the dynamics of a simplified reservoir network. Moreover, a simulation model of the nonlinear interfered spin wave confirmed that the system with the strongest nonlinearity under the present magnetic parameters gives the best performance for the reservoir tasks.[44] These effects were observed in other nanowire-base, photonic, or spintronic reservoir systems for the same reason: harnessing abundant nonlinearity from reservoirs results in good performance. In our case, the bias amplitude effect that led to a different nonlinear response of the network can enhance the extraction of relevant features from the reservoir. The achieved performance is compatible with other systems using a physical RC-based random network.[28,41] Furthermore, the majority of existing studies on nonlinear effect utilized self-organized nanowire networks, which contain fewer atomic switch junctions than nanoparticle networks with the same

functional area. As a result, it only provides partial atomic switch networks' learning ability. Our work opens the door for a thorough knowledge of the atomic switch network and offers up the possibility of adjusting the nanoparticle network's architecture and memristive response to enhance computing performance.

In conclusion, we presented an in-materio RC device fabricated using an Ag/Ag$_2$S NP network, which exhibits nonlinear dynamics initiated by atomic switch phenomena. We confirmed that stronger nonlinearity corresponded to better performance demonstrated by a sine-wave function approximation task. The results indicate that a higher bias voltage generates higher harmonic frequencies, which are essential for creating a high-dimensional space that facilitates linear regression. Moreover, in Boolean logic RC reconstruction, it was found that the nonlinear dynamics of the reservoir network was required for the logic operations by increasing the complexity of the nonlinear classifier (XOR vs OR). These findings provide insight into the principles of higher-performance information processing in RC. Ag/Ag$_2$S NPs exhibit nonlinear dynamic behavior that allows input signals to be mapped to a high-dimensional space, where linear classification or regression can be performed. This makes them a practical solution for implementing complex RC classification tasks such as voice or image classification. This is a promising area of research for the development of next generation machine-learning algorithms.

AUTHOR DECLARATIONS
Conflict of Interest

The authors have no conflicts to disclose.

Author Contributions

Thien Tan Dang: Data curation (lead); Formal analysis (lead); Investigation (lead); Methodology (lead); Visualization (lead); Writing – original draft (lead); Writing – review & editing (equal). **Oradee Srikimkaew:** Formal analysis (equal); Investigation (lead); Methodology (lead); Supervision (equal); Validation (equal); Visualization (equal). **Deep Banerjee:** Supervision (supporting); Visualization (supporting); Writing – review & editing (supporting). **Saman Azhari:** Resources (supporting); Software (lead); Visualization (supporting); Writing – review & editing (supporting). **Yuki Usami:** Formal analysis (supporting); Funding acquisition (supporting); Project administration (equal); Resources (equal); Supervision (equal); Visualization (equal); Writing – original draft (supporting); Writing – review & editing (supporting). **Hirofumi Tanaka:** Conceptualization (lead); Formal analysis (equal); Funding acquisition (lead); Project administration (lead); Resources (lead); Supervision (lead); Validation (lead); Writing – review & editing (lead).

DATA AVAILABILITY

The data that support the findings of this study are available from the corresponding author upon reasonable request.

REFERENCES

[1]H. Jaeger and H. Haas, Science **304**, 78 (2004).
[2]G. Tanaka, T. Yamane, J. B. Héroux, R. Nakane, N. Kanazawa, S. Takeda, H. Numata, D. Nakano, and A. Hirose, Neural Networks **115**, 100 (2019).
[3]S. Kan, K. Nakajima, Y. Takeshima, T. Asai, Y. Kuwahara, and M. Akai-Kasaya, Phys. Rev. Appl. **15**, 024030 (2021).
[4]K. Nakajima, Jpn. J. Appl. Phys., Part 1 **59**, 060501 (2020).
[5]K. Nakajima, H. Hauser, T. Li, and R. Pfeifer, Sci. Rep. **5**, 10487 (2015).
[6]R. Nakane, G. Tanaka, and A. Hirose, IEEE Access **6**, 4462 (2018).
[7]S. Tsunegi, T. Taniguchi, K. Nakajima, S. Miwa, K. Yakushiji, A. Fukushima, S. Yuasa, and H. Kubota, Appl. Phys. Lett. **114**, 164101 (2019).
[8]Y. Paquot, F. Duport, A. Smerieri, J. Dambre, B. Schrauwen, M. Haelterman, and S. Massar, Sci. Rep. **2**, 287 (2012).
[9]S. Sunada and A. Uchida, Sci. Rep. **9**, 19078 (2019).
[10]S. K. Bose, J. B. Mallinson, R. M. Gazoni, and S. A. Brown, IEEE Trans. Electron Devices. **64**, 5194 (2017).
[11]E. C. Demis, R. Aguilera, K. Scharnhorst, M. Aono, A. Z. Stieg, and J. K. Gimzewski, Jpn. J. Appl. Phys., Part 1 **55**, 1102B2 (2016).
[12]Y. Usami, B. Ven, D. G. Mathew, T. Chen, T. Kotooka, Y. Kawashima, Y. Tanaka, Y. Otsuka, H. Ohoyama, H. Tamukoh, H. Tanaka, W. G. Wiel, and T. Matsumoto, Adv. Mater. **33**, 2102688 (2021).
[13]S. Lilak, W. Woods, K. Scharnhorst, C. Dunham, C. Teuscher, A. Z. Stieg, and J. K. Gimzewski, Front. Nanotechnol. **3**, 675792 (2021).
[14]H. Ryu and S. Kim, Chaos, Solitons Fractals **150**, 111223 (2021).
[15]C. Lutz, T. Hasegawa, and T. Chikyow, Nanoscale **8**, 14031 (2016).
[16]A. Diaz-Alvarez, R. Higuchi, P. Sanz-Leon, I. Marcus, Y. Shingaya, A. Z. Stieg, J. K. Gimzewski, Z. Kuncic, and T. Nakayama, Sci. Rep. **9**, 14920 (2019).
[17]G. Milano, G. Pedretti, K. Montano, S. Ricci, S. Hashemkhani, L. Boarino, D. Ielmini, and C. Ricciardi, Nat. Mater. **21**, 195 (2022).
[18]X. Yan, Y. Pei, H. Chen, J. Zhao, Z. Zhou, H. Wang, L. Zhang, J. Wang, X. Li, C. Qin, G. Wang, Z. Xiao, Q. Zhao, K. Wang, H. Li, D. Ren, Q. Liu, H. Zhou, J. Chen, and P. Zhou, Adv. Mater. **31**, 1805284 (2019).
[19]H. Tanaka, M. Akai-Kasaya, A. Termehyousefi, L. Hong, L. Fu, H. Tamukoh, D. Tanaka, T. Asai, and T. Ogawa, Nat. Commun. **9**, 2693 (2018).
[20]D. Banerjee, T. Kotooka, S. Azhari, Y. Usami, T. Ogawa, J. K. Gimzewski, H. Tamukoh, and H. Tanaka, Adv. Intell. Syst. **4**, 2100145 (2022).
[21]M. Nakajima, K. Minegishi, Y. Shimizu, Y. Usami, H. Tanaka, and T. Hasegawa, Nanoscale **14**, 7634 (2022).
[22]T. Kotooka, S. Lilak, A. Stieg, J. Gimzewski, N. Sugiyama, Y. Tanaka, H. Tamukoh, Y. Usami, and H. Tanaka, *Ag2Se Nanowire Network as an Effective In-Materio Reservoir Computing Device* (2021).
[23]M. Hakoshima, Y. Usami, T. Kotooka, and H. Tanaka, Jpn. J. Appl. Phys., Part 1 **62**, SG1042 (2023).
[24]Hadiyawarman, M. Eguchi, and H. Tanaka, Jpn. J. Appl. Phys., Part 1 **59**, 015001 (2020).
[25]Hadiyawarman, Y. Usami, T. Kotooka, S. Azhari, M. Eguchi, and H. Tanaka, Jpn. J. Appl. Phys., Part 1 **60**, SCCF02 (2021).
[26]M. Brust, M. Walker, D. Bethell, D. J. Schiffrin, and R. Whyman, J. Chem. Soc., Chem. Commun. **7**, 801 (1994).
[27]C. Battocchio, C. Meneghini, I. Fratoddi, I. Venditti, M. V. Russo, G. Aquilanti, C. Maurizio, F. Bondino, R. Matassa, M. Rossi, S. Mobilio, and G. Polzonetti, J. Phys. Chem. C **116**, 19571 (2012).
[28]D. Banerjee, S. Azhari, Y. Usami, and H. Tanaka, Appl. Phys. Express **14**, 105003 (2021).

[29]K. Terabe, T. Hasegawa, T. Nakayama, and M. Aono, Nature **433**, 47 (2005).

[30]H. O. Sillin, R. Aguilera, H. H. Shieh, A. V. Avizienis, M. Aono, A. Z. Stieg, and J. K. Gimzewski, Nanotechnology **24**, 384004 (2013).

[31]A. Z. Stieg, A. V. Avizienis, H. O. Sillin, R. Aguilera, H. H. Shieh, C. Martin-Olmos, E. J. Sandouk, M. Aono, and J. K. Gimzewski, *Handbook of Memristor Networks*, 1st ed. (Springer, Cham, Switzerland, 2019), p. 391.

[32]H. Sun, Q. Liu, C. Li, S. Long, H. Lv, C. Bi, Z. Huo, L. Li, and M. Liu, Adv. Funct. Mater. **24**, 5679 (2014).

[33]Y.-J. Huang, S.-C. Chao, D.-H. Lien, C.-Y. Wen, J.-H. He, and S.-C. Lee, Sci. Rep. **6**, 23945 (2016).

[34]S. Nirantar, E. Mayes, M. A. Rahman, T. Ahmed, M. Taha, M. Bhaskaran, S. Walia, and S. Sriram, Adv. Electron. Mater. **5**, 1900605 (2019).

[35]L. Appeltant, M. C. Soriano, G. Van der Sande, J. Danckaert, S. Massar, J. Dambre, B. Schrauwen, C. R. Mirasso, and I. Fischer, Nat. Commun. **2**, 468 (2011).

[36]R. Zhu, S. Lilak, A. Loeffler, J. Lizier, A. Stieg, J. Gimzewski, and Z. Kuncic, Nat. Commun. **14**, 6697 (2023).

[37]M. Inubushi and K. Yoshimura, Sci. Rep. **7**, 10199 (2017).

[38]A. V. Avizienis, H. O. Sillin, C. Martin-Olmos, H. H. Shieh, M. Aono, A. Z. Stieg, and J. K. Gimzewski, PLoS One **7**, e42772 (2012).

[39]K. Liu, B. Dang, T. Zhang, Z. Yang, L. Bao, L. Xu, C. Cheng, R. Huang, and Y. Yang, Adv. Mater. **34**, 2108826 (2022).

[40]S. Azhari, D. Banerjee, T. Kotooka, Y. Usami, and H. Tanaka, Nanoscale **15**, 8169 (2023).

[41]T. Chen, J. van Gelder, B. van de Ven, S. V. Amitonov, B. de Wilde, H.-C. Ruiz Euler, H. Broersma, P. A. Bobbert, F. A. Zwanenburg, and W. G. van der Wiel, Nature **577**, 341 (2020).

[42]S. K. Bose, C. P. Lawrence, Z. Liu, K. S. Makarenko, R. M. J. van Damme, H. J. Broersma, and W. G. van der Wiel, Nat. Nanotechnol. **10**, 1048 (2015).

[43]K. I. Kitayama, M. Notomi, M. Naruse, K. Inoue, S. Kawakami, and A. Uchida, APL Photonics **4**, 090901 (2019).

[44]W. Namiki, D. Nishioka, Y. Yamaguchi, T. Tsuchiya, T. Higuchi, and K. Terabe, Adv. Intell. Syst. **5**, 2300228 (2023).

22 July 2024 06:37:51